GPS Solut (2018) 22:8
https://doi.org/10.1007/s10291-017-0666-x

ORIGINAL ARTICLE

S_4 index: Does it only measure ionospheric scintillation?

Gabriela de Oliveira Nascimento Brassarote[1] · Eniuce Menezes de Souza[2] · João Francisco Galera Monico[1]

Received: 14 June 2016 / Accepted: 13 October 2017 / Published online: 6 November 2017

Abstract The study of ionospheric scintillation has played a critical role in ionospheric research and also in satellite positioning. This is due to the growing influence of GNSS in navigation and remote sensing activities and also because the scintillation severely degrades the performance of this system. The main parameter that has been used to investigate the ionospheric scintillation impact on quality of GNSS satellite signals is the S_4 index. However, we show that other effects such as multipath may mask the scintillation effects. Furthermore, we propose a method to separate the effect of multipath from scintillation in the S_4 index by a non-decimated wavelet multiscale decomposition, which is shift invariant and more appropriate to use in the analysis of time series. The results show that the multipath effect is evident in the smoother scales of multiscale decomposition by wavelet in the weak scintillation period. Once identified and estimated, this effect can be removed from the S_4 index series during strong scintillation periods and it becomes not significant in the scintillation S_4 index wavelet analysis. Investigations using data from different stations and satellites demonstrate that the effect of ionospheric scintillation varies with station location and elevation angle of the satellite. Therefore, each case must be treated individually.

Keywords Ionospheric scintillation · GNSS · Wavelets

Introduction

The GNSS (global navigation satellite system) has become a useful and indispensable technology for positioning and timing. However, several effects influence the signal along its path from the satellite to the receiver. This is because the GNSS signals propagate through the earth's atmosphere, through layers of different types and densities. Thus, the satellite signals encounter different forms of influences, which may cause variations in direction and velocity propagation, polarization, and power. These effects can degrade the quality of the GNSS observable and the accuracy of positioning.

The ionosphere is one of the largest sources of interference in the propagation of GNSS signals. The ionospheric scintillation, caused by irregularities in the electron density, can weaken the signal received by the GNSS receiver, causing degradation of positioning or even signal loss (McNamara 1991).

The effects of ionospheric scintillation are more severe in the equatorial and low-latitudes regions, as well as in the high-latitudes regions, especially at the poles (Kintner et al. 2007; Davies 1990). The scintillation events in high latitudes are related to the periods of high solar activity and magnetic storms. On the other hand, in the equatorial and low-latitudes regions, the scintillation events occur mainly due to equatorial ionization anomaly (EIA) and ionospheric bubbles that are formed in this region soon after sunset (Kelley 1989).

✉ Gabriela de Oliveira Nascimento Brassarote
gabrielabrassarote@gmail.com

Eniuce Menezes de Souza
emsouza@uem.br

João Francisco Galera Monico
galera@fct.unesp.br

[1] São Paulo State University – UNESP-Brazil, Roberto Simonsen, 305, Presidente Prudente, São Paulo State 19060-900, Brazil

[2] Maringa State University - UEM –Brazil, Colombo Av., 5790, Maringá, Parana State 87020-900, Brazil

For high-latitude regions, the scintillation has been well characterized in the literature. Indeed, some studies applying wavelets have contributed in deriving scintillation indexes by wavelet detrending methods instead of the Butterworth filters traditionally used in receivers (Materassi et al. 2009; Mushini et al. 2012; Tiwari et al. 2011, 2013). We are using the S_4 index obtained by detrending the raw high-rate-intensity measurements using a low-pass Butterworth filter with a cutoff frequency of 0.1 Hz.

Using the available S_4 index, which measures the amplitude scintillation, we performed a multiscale analysis by wavelets to obtain a more realistic S_4 index and to investigate the scintillation effect on the Global Positioning System (GPS) signals. Experiments were carried out in different locations of Brazil. The main purpose is to evaluate the presence of other contributions to the S_4 scintillation index and thus to estimate and separate them from S_4. The periodic behavior of "U" shapes seen in the time series of the S_4 index indicates that some cyclic effects are included in the S_4 scintillation index, which are probably related to effects such as multipath. This "U" shape of periodic behavior is because the elevation angle of the satellite follows a shape of inverted "U" and the reflections and noise are more pronounced at lower angles, i.e., the lower the elevation angle of the satellite, the greater the multipath effect. For a complete multiscale analysis of the S_4 index, we use the non-decimated discrete wavelet transform (NDWT). Initial results using NDWT in this sense have been promising (Brassarote et al. 2015). This transform is more adequate to time series than the decimated discrete wavelet transform which is mostly used in literature. The NDWT is translation invariant and keeps the same number of coefficients in each scale, corresponding to all time instants at which the data are collected. The temporal correspondence makes, for instance, multipath repeatability quite easy to be identified in different scales. Thus, information and hidden patterns that could not be detected in the time or frequency domain can be explained more clearly in the time–frequency domain.

We first give a brief overview of ionospheric scintillation, and we present the multiscale decomposition method by NDWT used in our scintillation S_4 index analysis. We then present how the experiments were carried out and how the methodology was applied to estimate and separate sidereal-day effects from scintillation in S_4 index. The results obtained from the proposed methodology as well as the analysis of the scintillation S_4 index before and after removal of the estimated sidereal-day effect are presented after that. Final considerations are presented at the end.

Theoretical aspects

We briefly explain the effects of ionospheric scintillation on GNSS positioning and the multiscale decomposition from non-decimated wavelets used to assess the S_4 index time series of scintillation. We explain the reason for using wavelets in the real signal analysis instead of Fourier-based methods, and we highlight the advantages of applying the NDWT for a complete multiscale analysis of scintillation time series. The description of the NDWT pyramidal algorithm and the method used to calculate the NDWT are given in Appendix.

Ionospheric scintillation and its effects in the GNSS positioning

The ionosphere is a layer of the atmosphere located between 50 and 1000 km of altitude, formed by the interaction of sunlight with different gases that constitute the atmosphere (McNamara 1991). The effect of the ionosphere depends on the frequency and the refractive index. The latter is proportional to the TEC (total electron content), i.e., the number of electrons along the path from satellite to receiver. The TEC varies in time and space, depending on solar radiation, geomagnetic activity, sunspot cycle, season, user location and direction between the satellite and the receiver (Camargo et al. 2000). In addition, in the ionosphere there are anomalies and irregularities which affect the propagation of GNSS signal, such as the equatorial anomaly, ionospheric bubbles and ionospheric scintillation (Maini and Agrawal 2007; Kintner et al. 2007).

Ionospheric scintillation can be described as a rapid change in phase and amplitude of the GNSS signal when it passes through irregularities in electron density along its path (Kintner et al. 2001). It is more intense in the equatorial and low-latitudes regions and high latitudes (Kintner et al. 2007). Brazil, which has much of its territory located in the equatorial region, is strongly affected by the scintillation occurrence.

The intensity of scintillation effects in Brazilian longitudes varies seasonally. The strongest scintillation occurs from September to March, while the minimum effects take place during April to August (Camargo et al. 2000). Regarding daily variations, ionospheric irregularities intensify at night, more specifically after sunset with duration of 5 to 6 h. The incidence of ionospheric scintillation plus the weak coverage of satellites can lead to loss of positioning service, compromising the performance of activities such as air navigation and precision agriculture.

Due to the seemingly random and uncorrelated nature, modeling the ionospheric scintillation has not been feasible. However, through some quantitative information of the scintillation, as the S_4 and phi60 (or sigma-phi–σ_φ) indexes, it is possible to characterize and understand the ionospheric

irregularities that cause ionospheric scintillation (Kintner et al. 2007).

The S-value is a way to characterize the power variation of a signal over time. The S_4, i.e., the fourth harmonic index and most used one among all S indexes, maps the intensity of ionospheric scintillation. The σ_φ index shows the variation of the carrier phase measurement φ at the receiver during the past 60 s, i.e., it quantizes the standard deviation of the GPS signal phase (Streets 1969; Briggs and Parkin 1963).

The S_4 index is defined by the standard deviation of the received signal power normalized to average signal power (Briggs and Parkin 1963). According to Tiwari et al. (2011), this index can be classified into mutually exclusive categories depending directly on the signal intensity that occurred on the day and place in question: strong ($S_4 \geq 1.0$), moderate ($0.5 \leq S_4 \leq 1.0$) and weak ($0 \leq S_4 \leq 0.5$).

Multiscale decomposition from non-decimated wavelets

Transforms are applied to signals to obtain more information about them, which are not readily available in the original signal. The transformation of a signal from the time domain to the frequency domain can be done through several mathematical tools, of which the best known is probably the Fourier transform (FT). The basic principle of the FT is to represent a periodic signal as the sum of sines and cosines. These sine waves are well located in frequency but not in time, because their support is of infinite length. Therefore, the FT allows the identification of the signal frequencies but the time information is completely lost in the transformed signal. Thus, the FT is only suitable for stationary signals, i.e., signals whose frequency does not change over time. This is not the case for real signals, which are usually non-stationary.

One possibility is to apply the windowed Fourier transform (WFT), which uses a fixed-length and sliding window to calculate the FT, assuming the signal has stationary behavior inside each window. This application would solve the frequency localization problem, but it would depend on the length of the window used. In addition, another problem of the WFT is the inconsistent treatment of different frequencies. In the low frequencies, there are so few oscillations within the window that the frequency location is lost, whereas in the high frequencies there are so many oscillations that the time location is lost. Therefore, it is necessary to apply a transform with a window of variable length. This is the basic idea of the wavelet transform (WT), which expands a function using a set of wavelet functions that have time–frequency location.

A wavelet expansion uses translations and dilations of a function called mother wavelet ψ, allowing one to obtain a family of functions (Nason 2008),

$$\psi_{a,b}(x) = \frac{1}{\sqrt{|a|}}\psi\left(\frac{x-b}{a}\right), \quad a, b \in R, \quad a \neq 0 \tag{1}$$

where a is the dilation factor and b the translation factor. Considering $a = 2^{-j}$ and $b = k2^{-j}$, $j \in R$, there is a function ψ with time–frequency location such that $\psi_{j,k}(x) = 2^j\psi(2^j x - k)$ is an orthonormal basis for the space $L^2(R)$.

So, the discrete wavelet transform (DWT) of a time series X_t with relation to mother wavelet ψ is

$$W_{j,k} = \sum_{t=0}^{n-1} X_t \psi_{j,k}(t) \tag{2}$$

where $n = 2^{j_0}$ is the number of observation of the time series X_t, $j = 0, \ldots, j_0 - 1$ and $k = 0, \ldots, 2^{j_0-1}$ with $j_0 \in Z$. The first decomposition level is going to be related to the smallest scale representing the effects of highest resolution level or highest frequency. The greater the decomposition level, the lower the frequency representing the greatest and smoothest scales.

This is the version of WT most well known, which is also calculated through the pyramidal algorithm developed by Mallat (1989). This process uses discrete filters and downsampling, where for each two outputs of the filter one output is discarded, resulting in each stage of the algorithm having half of the elements considered in the previous stage. However, the downsampling required for DWT calculation makes it sensitive to the origin, which is not ideal for some applications, mainly those involving non-stationary time series analysis.

On the other hand, the NDWT is shift invariant because it considers all the elements of the sample by eliminating the downsampling and, consequently, represents a time series with the same number of coefficients at each decomposition level of the pyramidal algorithm. Thus, the use of the NDWT allows a complete analysis in multiscale of the time series identifying the frequency of occurrence and location in time of severe non-stationarity caused by spikes of different magnitudes. In addition, the NDWT makes a reliable approximation of the magnitude of these effects. The NDWT pyramid algorithm is presented in Appendix.

The wavelet periodogram decomposes the energy, or variance, of the time series $\{X_t\}$ in 2^j multiscale, i.e., different levels of resolution j and with time–frequency location $2^j t$ (Nason 2008). It is calculated from the NDWT wavelet coefficients, being described by

$$I_{j,t} = \left|\tilde{W}_{j,t}\right|^2 \tag{3}$$

where $\tilde{W}_{j,t}$ is calculated by (5) presented in Appendix. Note that $\tilde{W}$ is the non-decimated version of the decimated wavelet transform W, obtained in (2).

The wavelet periodogram gives a good description of where significant changes are located in the time series because abrupt changes in the series correspond proportionately to coefficients of large magnitude.

The sum of all NDWT wavelet coefficients at each scale of the periodogram allows calculating the variance of the time series at each scale. This task is executed by the global wavelet spectrum, using the following equation

$$S_{j,t} = \frac{1}{N}\sum_{n=0}^{N-1}\left|\tilde{W}_{j,t}\right|^2 \quad (4)$$

The global wavelet spectrum completes the multiscale (or multiresolution) analysis of time series. From the periodogram, the scale that has the most energy and characterizes the time series better can be identified. Table 1 provides a resolution interpretation of wavelet decomposition for S_4 index in minutes by decomposition level j and scale $\tau_j = 2^{j-1}$ (Percival and Walden 2000).

Each scale τ_j related to decomposition level j corresponds to a period interval from $2\tau_j$ to $4\tau_j$. As the data are at minute intervals, resolution interpretation of each scale is given in minutes, hours and days. The greater the decomposition level j, the greater the scale τ_j. So, the effects related to this scale have low frequency.

Experiments

To investigate the effect of ionospheric scintillation on GPS signals in different regions of Brazil through the S_4 index, we used the database of the CIGALA/CALIBRA (Concept for Ionospheric Scintillation Mitigation for Professional GNSS in Latin America/Countering GNSS high Accuracy applications Limitations due to Ionospheric disturbances in BRAzil) project available through the ISMR Query Tool developed in the São Paulo State University in Presidente Prudente (FCT-UNESP), Brazil (Vani et al. 2016). Figure 1 shows the locations of the 12 stations used, which have data available from Septentrio PolaRxS Pro receivers since February 14, 2011. The PolaRxS Pro receivers can generate and store raw data at high rate of 50 Hz in hourly files which can be processed to provide scintillation indices S_4 and σ_φ, among others (Vani et al. 2016).

The selected stations to perform the analysis are MAN2 (data available until 2014—this station was replaced by MAN3 after 08/07/2014), PALM, POAL, PRU1 and SJCU in the cities of Manaus, Palmas, Porto Alegre, Presidente Prudente and São José dos Campos, respectively. They were chosen according to their geographical location to provide an evaluation of the ionospheric scintillation effect from different positions in relation to the geomagnetic equator.

To evaluate the ionospheric scintillation effect on GPS signals at different times of the year 2013, data from

Table 1 Frequency and period interval in each scale $\tau_j = 2^{j-1}$

Decomposition level	Scale	Frequency interval	Period interval in minutes
j	τ_j	$\left(\frac{1}{4\tau_j}, \frac{1}{2\tau_j}\right]$	$[2\ \tau_j, 4\tau_j)$
1	$\tau_1 = 1$	$\left(\frac{1}{4}, \frac{1}{2}\right]$	2–4 min
2	$\tau_2 = 2$	$\left(\frac{1}{8}, \frac{1}{4}\right]$	4–8 min
3	$\tau_3 = 4$	$\left(\frac{1}{16}, \frac{1}{8}\right]$	8–16 min
4	$\tau_4 = 8$	$\left(\frac{1}{32}, \frac{1}{16}\right]$	16–32 min
5	$\tau_5 = 16$	$\left(\frac{1}{64}, \frac{1}{32}\right]$	32 min–1 h 4 min
6	$\tau_6 = 32$	$\left(\frac{1}{128}, \frac{1}{64}\right]$	1 h 4 min–2 h 8 min
7	$\tau_7 = 64$	$\left(\frac{1}{256}, \frac{1}{128}\right]$	2 h 8 min–4 h 16 min
8	$\tau_8 = 128$	$\left(\frac{1}{512}, \frac{1}{256}\right]$	4 h 16 min–8 h 32 min
9	$\tau_9 = 256$	$\left(\frac{1}{1024}, \frac{1}{512}\right]$	8 h 32 min–17 h 4 min
10	$\tau_{10} = 512$	$\left(\frac{1}{2048}, \frac{1}{1024}\right]$	17 h 4 min–1 day 14 h 8 min
11	$\tau_{11} = 1024$	$\left(\frac{1}{4096}, \frac{1}{2048}\right]$	1 day 14 h 8 min–2 day 20 h 16 min

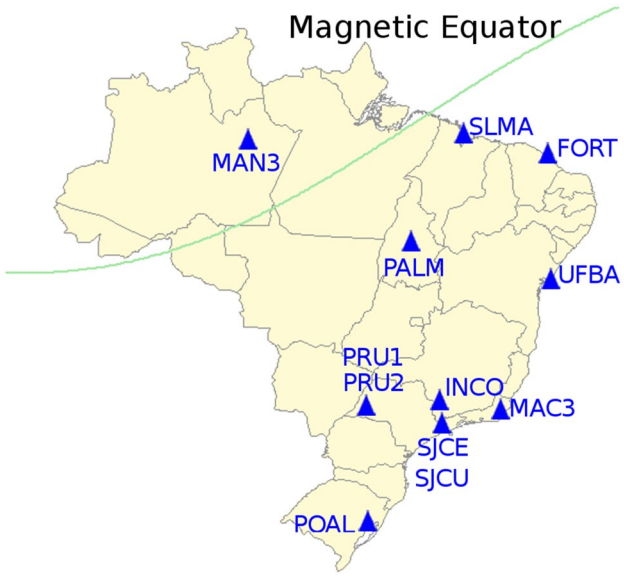

Fig. 1 Distribution of stations of the CIGALA/CALIBRA network in Brazil, 2016

March and June within considered periods of, respectively, strong and weak scintillation were selected (Camargo et al. 2000). For a better visualization of data and results, we use 6 days of data in each period (March and June).

When estimating the multipath effect, the S_4 index time series on weak scintillation effect were decomposed in multiscale by the Symlets wavelet family with 10 vanishing moments (SYM10). To identify this optimal wavelet base, a comparison was carried out of Daubechies with 6, 8 and 10 vanishing moments (DAUB6, DAUB8, DAUB10), Symlets with 4, 6, 8 and 10 vanishing moments (SYM4, SYM6, SYM8, SYM10), and Starlet bases. The Starlet wavelet, also an undecimated wavelet, has been widely used in astronomical applications (Starck et al. 2011). A reason that motivates the use of Starlet wavelet here is that it does not require orthogonal or biorthogonal filters and offers easy and fast computing, besides to being ideal for handling large data size such as the ionospheric scintillation data.

The results of the application of the three wavelet bases on the S_4 scintillation signals were all very similar, showing that in this case there is no problem in selecting a different base. Therefore, we decided to apply the well-known Symlets wavelet with 10 vanishing moments for this application.

From multiscale analysis, one can check for the presence of periodic effects in the scintillation index and their relationship with the scale of the wavelet periodogram. Thus, analyzing more than 2 days of data one can check the presence of cyclic effects such as daily repeatability.

Repeatability in the scale that represents the sidereal-day effects is mainly attributed to multipath, being the effect that repeats daily according to the satellite motion if the receiver environment remains unchanged.

Once periodic effects have been detected from the wavelet periodogram, the scale corresponding to them can be rebuilt to estimate the sidereal-day effect in the time domain. We proposed to estimate the sidereal-day multipath effect in the weak scintillation period, avoiding overestimating these effects. Considering the repeatability of the multipath effect, the goal is to remove it from the strong scintillation period.

Through the above procedure, it is possible to separate scintillation effect from other sidereal-day effects, mainly multipath, that may influence the S_4 index, and thus provide an index that better represents the ionospheric scintillation. The implementation was performed in R language (http://cran.r-project.org/), wherein open code routines such as packages "wavethresh" and "tseries" were used.

Results and analysis

The procedure of separating the multipath effect from the scintillation index was applied as described above to GPS satellites 1, 11, 19 and 31 in each of the five selected stations of the CIGALA/CALIBRA network. However, the results are illustrated for PRN 11 satellite in the stations most (PRU1) and least (MAN2) affected by ionospheric scintillation. PRN 11 was chosen due to high ionospheric scintillation intensity on S_4 index for this satellite. The comparison between stations PRU1 and MAN2 allows illustrating the presence of spatial variability. On the other hand, GPS satellite 31 is used to illustrate the comparison of the scintillation effect between satellites at the same station, in this case station PRU1. Nevertheless, discussions will be extended to all stations and satellites in which the procedure was applied.

As mentioned previously, the purpose of decomposing the S_4 index time series of the weak scintillation period in multiscale is to estimate the effect of multipath and then remove it from a strong scintillation period in an attempt to separate the multipath and scintillation effects. This process will be presented in the next sections.

Estimation of the sidereal-day effect in weak scintillation period

First, the S_4 time series that characterize weak ionospheric were analyzed graphically. The time series relative to GPS satellite 11 at stations MAN2 and PRU1 and GPS satellite 31 at station PRU1 can be seen in each top-left panel in Figs. 2, 3 and 4. The S_4 time series show gaps caused by the lack of data, when the satellites are not being tracked, and a daily behavior that is mostly related to multipath effect. In each of the 6 days of data, the GPS satellites 1, 11 and 19 were tracked by the receiver on the time of the

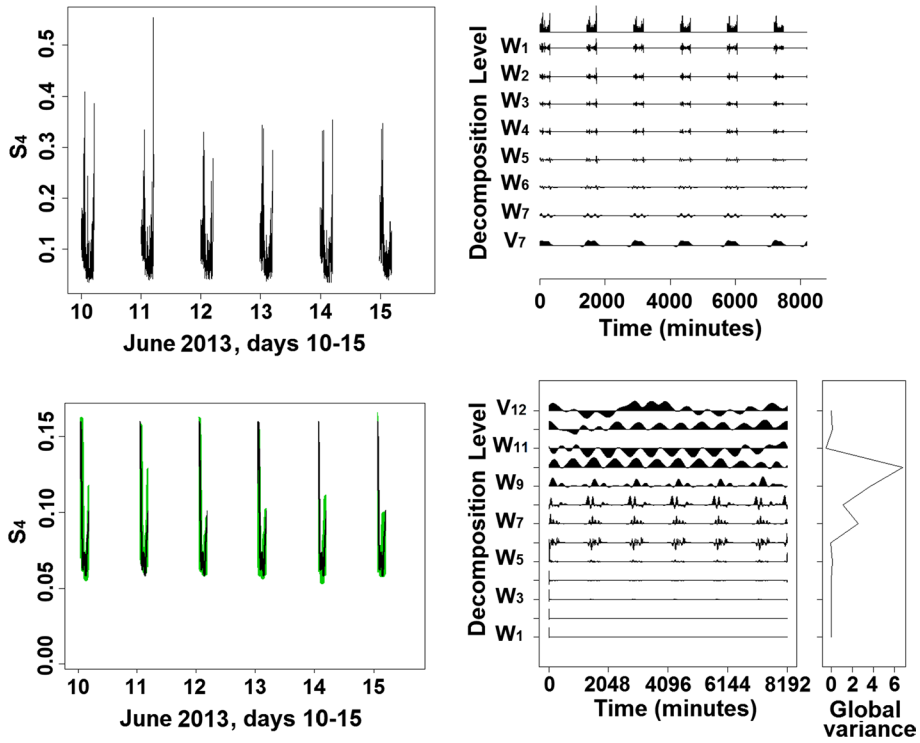

Fig. 2 Estimation of the sidereal-day effect for GPS satellite PRN 11 and station MAN2. S_4 time series of weak ionospheric scintillation period (top-left), multiscale decomposition by Symlets wavelet (top-right), estimation of the sidereal-day effect (green) and average sidereal-day effect (black) (bottom-left), and periodogram of the average sidereal-day effect estimated (bottom-right). W_j indicates the wavelet coefficients like those from Eq. (2) but applying NDWT (Eq. 7 Appendix) while the V_j represents those related to the lowest frequency or smoothest part (Eq. 8 Appendix)

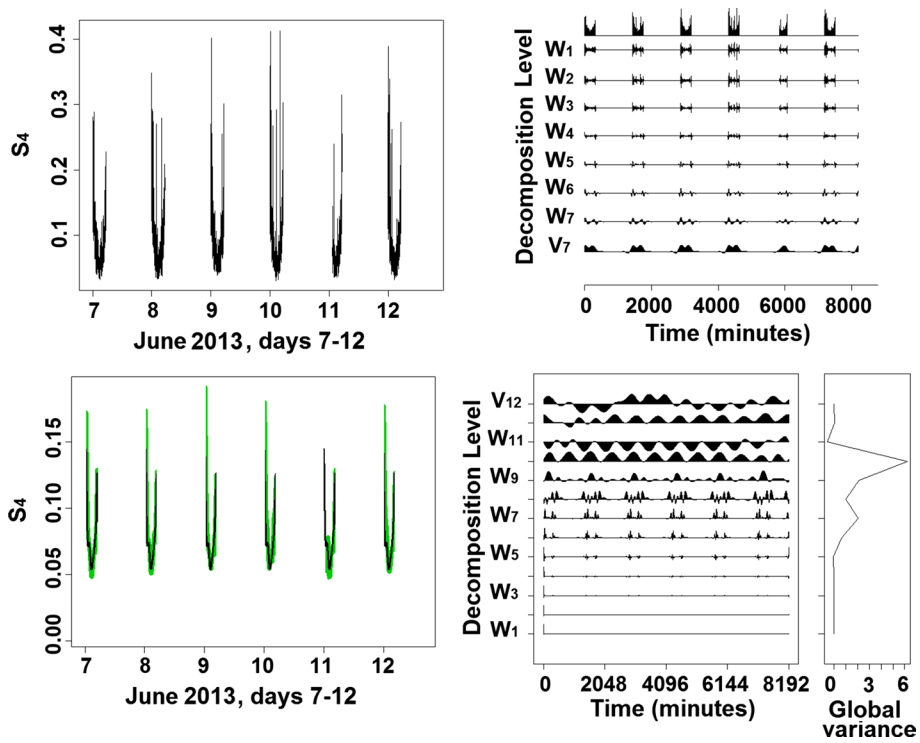

Fig. 3 Estimation of the sidereal-day effect for GPS satellite 11 and station PRU1. S_4 time series of weak ionospheric scintillation period (top-left), multiscale decomposition by Symlets wavelet (top-right), estimation of the sidereal-day effect (green) and average sidereal-day effect (black) (bottom-left), and periodogram of the average sidereal-day effect estimated (bottom-right)

day from 16 h UTC to 23 h UTC on analyzed stations. GPS satellite 31, on the other hand, was visible twice per day tracked by the receiver from 16 h UTC to 20 h UTC and from 9 h UTC to 12 h UTC. The daily behavior is "U-shaped," whereas the satellite elevation angle follows a shape of inverted "U," what is expected since the reflections (multipath) and noises are more expressive at lower elevation angles, as shown Fig. 5. The presence of these effects in the time series may influence the analysis of the ionospheric scintillation index.

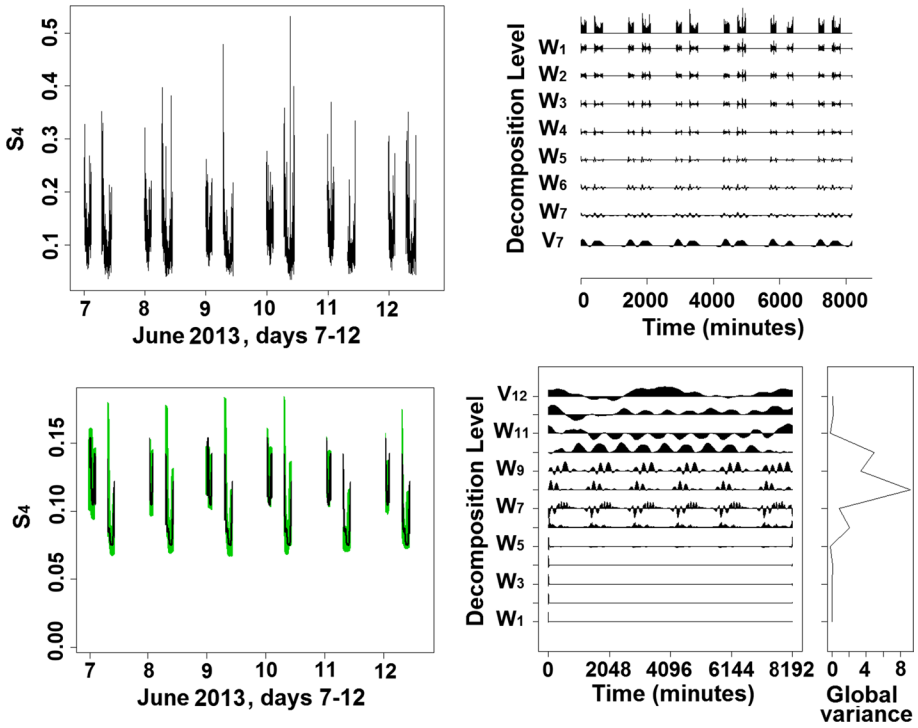

Fig. 4 Estimation of the sidereal-day effect for GPS satellite 31 and station PRU1. S_4 time series of weak ionospheric scintillation period (top-left), multiscale decomposition by Symlets wavelet (top-right), estimation of the sidereal-day effect (green) and average sidereal-day effect (black) (bottom-left), and periodogram of the average sidereal-day effect estimated (bottom-right)

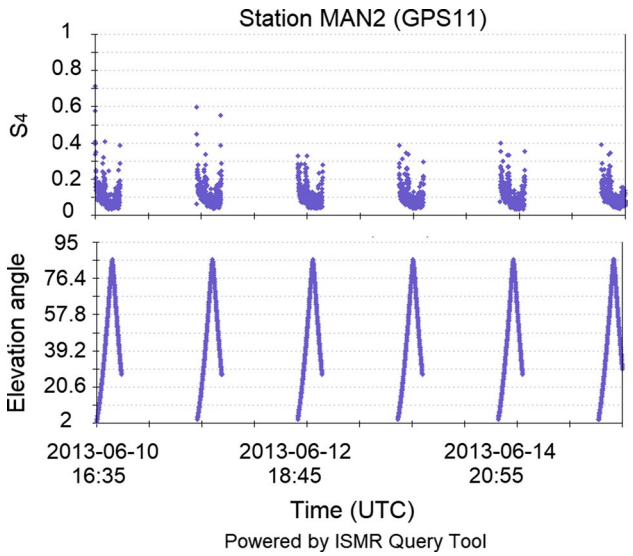

Fig. 5 S_4 index time series (top) and elevation angles (bottom) for GPS satellite 11 at station MAN2 station

Thus, the multiscale method described above was applied to S_4 time series of GPS 11 satellite in station MAN2 during the weak ionospheric scintillation period (top-left panel, Fig. 2). In this multiscale decomposition of the consolidated 6 days of data, it is possible to analyze which scale has repeatability in periods when there is data, that is, which ones show the periodic behavior present in the scintillation index. Such scales are those that must be reconstructed for the estimation of the periodic effect, i.e., the multipath. In the analyses carried out, the weak scintillation data are decomposed into seven levels (top-right panel, Fig. 2). The decomposition levels 6 and 7 present periodic behavior data, as can be seen in Fig. 6; therefore, they should be reconstructed.

Since multipath is an effect that repeats on consecutive days, it is interesting to estimate a single average effect that describes this behavior in the scintillation data. Whereas the S_4 data have a different behavior for each satellite and station, even referring to the same period of data, it is necessary

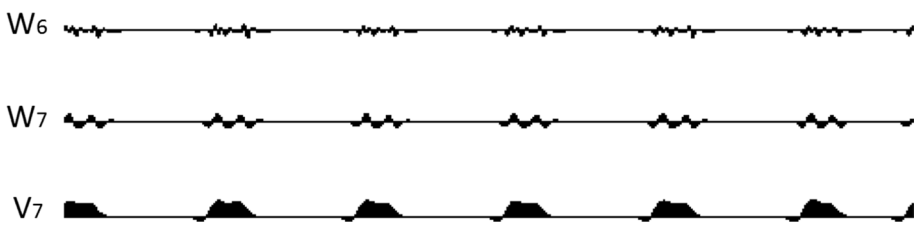

Fig. 6 Zoom of decomposition levels 6 and 7 of wavelet decomposition shown in top-right panel (Fig. 2). The figure shows periodicity present in the S_4 time series

to estimate an average function that describes the multipath, specific to each satellite and each station. This is obtained in the bottom-left panel in Fig. 2 by the average (in black) of the 6 days of data characterizing multipath. The periodogram of the average estimated sidereal-day effect as well as the wavelet global spectrum are presented in the bottom-right panel in Fig. 2.

Figures 3 and 4 show the results for the estimation of the sidereal-day effect (multipath) related to GPS satellites 11 and 31 for station PRU1 (top-left panels) and multiscale decomposition of the S_4 time series that characterize weak ionospheric scintillation (top-right panels). Once the scales with the daily repeatability were verified (scales of 6 and 7 decomposition levels), the estimation of the sidereal-day effect was obtained by the reconstruction of these scales, which can be seen in green in the bottom-left panel in each figure. Once there is a natural variability in the daily repeatability of observed time series, an average sidereal-day effect was estimated and plotted in black in these figures (also bottom-left panel). Periodogram of the average estimated sidereal-day effect and the wavelet global spectrum are presented in the bottom-right panels.

For GPS satellite 11 of all analyzed stations, the estimated periodic behavior turns out to be the same, since in all cases the most expected scale in the wavelet periodogram is the one of decomposition level 10. This scale is related to the daily repeatability, as can be seen in Table 1. It is also more expressive, i.e., it presents greater global variance. The periodogram of the ionospheric scintillation S_4 time series illustrated in top-right panel in Figs. 7 and 8 shows how this sidereal-day periodic effect influences the S_4 index analysis. Similarly, all satellites of station PRU1 show the decomposition level 10 as the most evident (the greatest global variance), except PRN 31. The sideral-day repeatability is represented by the second spike for PRN 31 (bottom-right panel, Fig. 4), because 2 shapes of "U" occur in each day (due to the fact that satellite is visible twice each day–span of just over 4 h). The scale related to the 8th decomposition level became more evident.

Removal of sidereal-day effect (multipath) in strong scintillation period

Once the multipath was estimated during the period of low scintillation effects, the proposed method is to remove it from the scintillation data during the period of strong scintillation effect. The removal was done in the time domain, by subtracting the estimated multipath effect of the S_4 time series. The series obtained in the bottom-left panels of Figs. 7, 8 and 9 have minor influence of periodic effects. For a more detailed analysis in multiscale of the scintillation time series before and after the multipath removal, we evaluated the wavelet spectrum estimated by the wavelet periodogram and the global spectrum that represents the energy or the total variance of the series at each decomposition level (or scale). The results can be visualized in top-right panels and bottom-right panels of Figs. 7, 8 and 9.

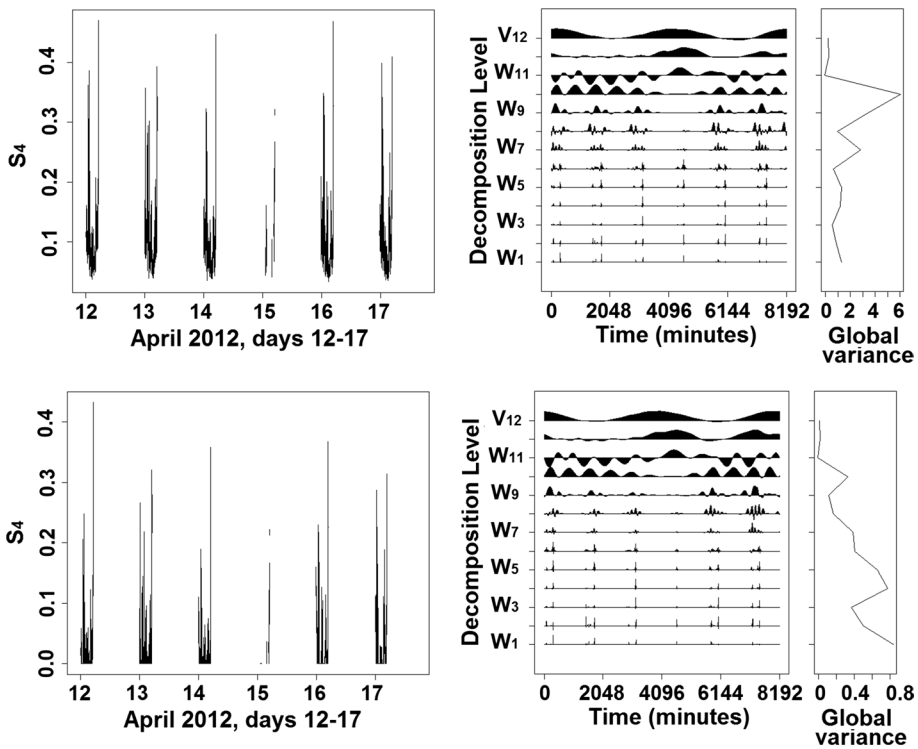

Fig. 7 Multiscale analysis of GPS satellite PRN 11 and station MAN2. S_4 index time series of weak ionospheric scintillation period before (top-left) and after (bottom-left) removal of sidereal-day effect, periodogram of time series without (top-right) and with (bottom-right) removal of average estimated sidereal-day effect

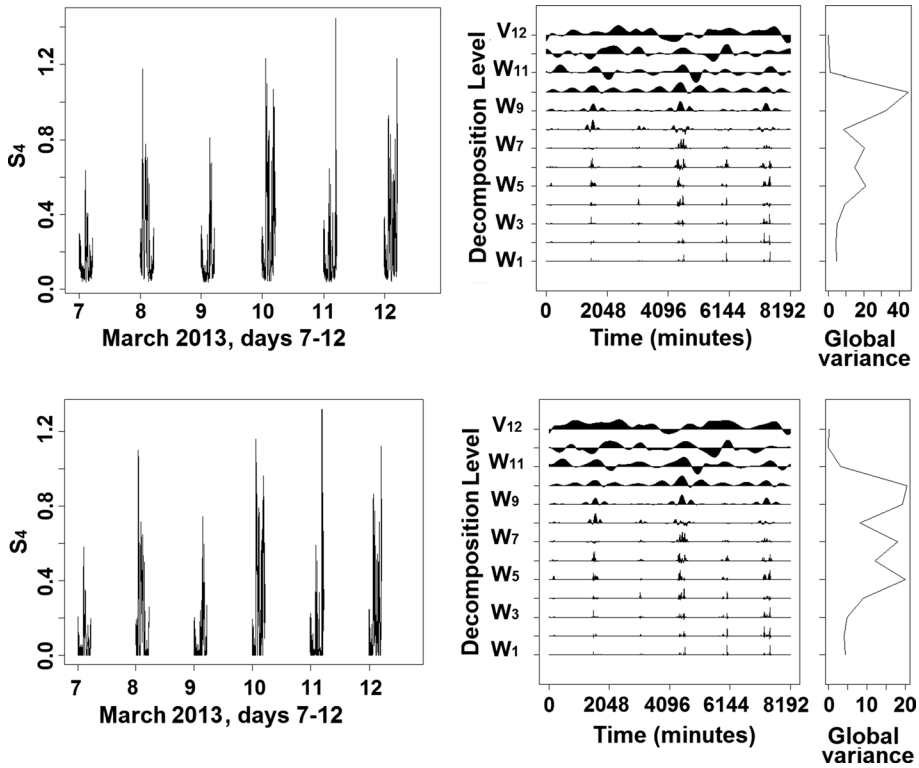

Fig. 8 Multiscale analysis of GPS satellite PRN 11 and station PRU1. S_4 index time series of weak ionospheric scintillation period before (top-left) and after (bottom-left) removal of sidereal-day effect; periodogram of time series without (top-right) and with (bottom-right) removal of average estimated sidereal-day effect

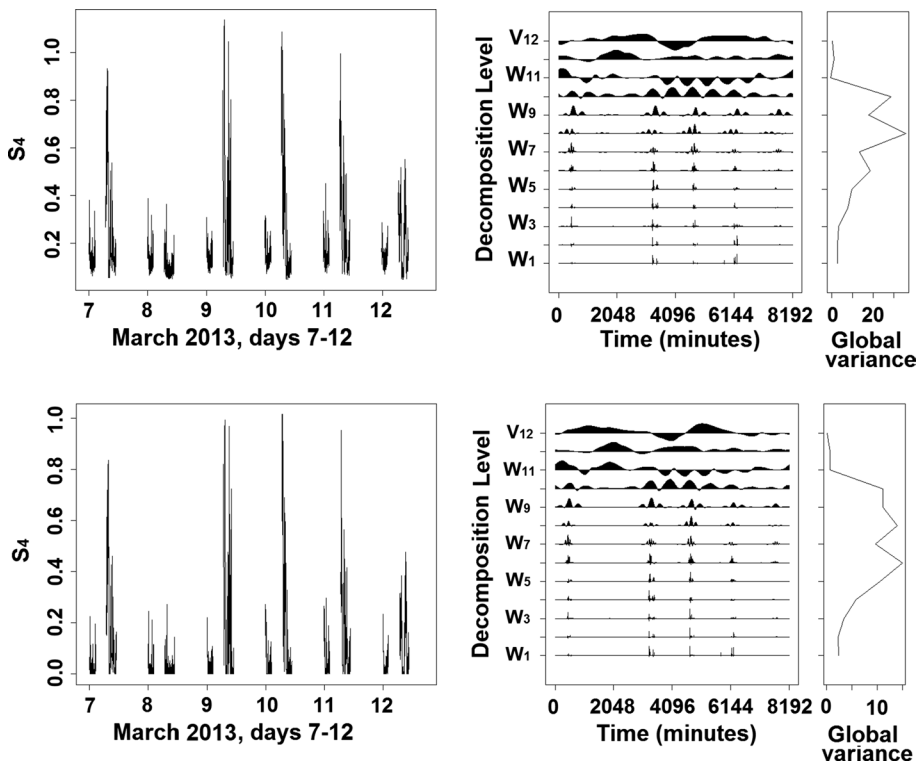

Fig. 9 Multiscale analysis of GPS satellite PRN 31 and station PRU1. S_4 index time series of weak ionospheric scintillation period before (top-left) and after (bottom-left) removal of sidereal-day effect; periodogram of time series without (top-right) and with (bottom-right) removal of average estimated sidereal-day effect

By the analysis of Figs. 7, 8 and 9 and comparison of the periodogram plotted in top-right and bottom-right panels, it is observed that with the multipath removal there was a change in the scale with the highest concentration of energy (global variance). This means that having removed the multipath effect of the series, this periodic effect, mainly

concentrated in the scale of decomposition level 10, is no longer the most significant in the spectrum.

It is evident in the wavelet analysis, that by observing the periodograms of S_4 index scintillation with removal of sidereal-day effect (bottom-right panels, Figs. 7, 8 and 9), the scales that explain better the scintillation time series for PRN 11 are those of decomposition levels 9 for station SJCU, 8 for PALM, 4 for POAL and MAN2, and decomposition level 5 for PRU1. Such scales are related to the effects from 8 to 17 h, 4 to 8 h, 16 to 32 min and from 32 min to 1 h, respectively, confirming that the effects of scintillation change with the station location. Note also that the most evident scale of the periodograms changes according to the analyzed GPS satellite. In the case of station PRU1, these main scales change to 5 for PRN 1 and PRN 11 (bottom-right panel, Fig. 8), to 8 for PRN 19 and to 6 for PRN 31 (bottom-right panel, Fig. 9). This shows that the scintillation frequency behaviors are different for each satellite at different elevation angles, indicating that it needs to be treated individually.

Comparison of S_4 index among the stations

Regarding the comparison of scintillation index in the time domain, Fig. 10 shows the box plots for the S_4 index data, during the 6-day period of strong scintillation effect, at different times to each station, before and after removal of multipath. Although the dataset had not been collected in same time for all stations, it is available to the same period of March or April (strong scintillation period) making it possible to compare the results. The figure shows that after removal of multipath in the S_4 index, the median is reduced for all stations. From the Wilcoxon test, considering a significance level of 5%, the null hypothesis of equal medians could be rejected for S_4 index of all stations (p value < 0.001) confirming the reduction of the median, which were 0.09 for the stations MAN2 and PRU1, 0.07 for SJCU and PALM and 0.06 for station POAL. Furthermore, the distribution became more asymmetric toward the right. Besides the visualization of the box plots, the skewness coefficients, a measure of symmetry estimated by the expectation $E\left[\left(\frac{x-\mu}{\sigma}\right)^3\right]$, can be seen in Table 2.

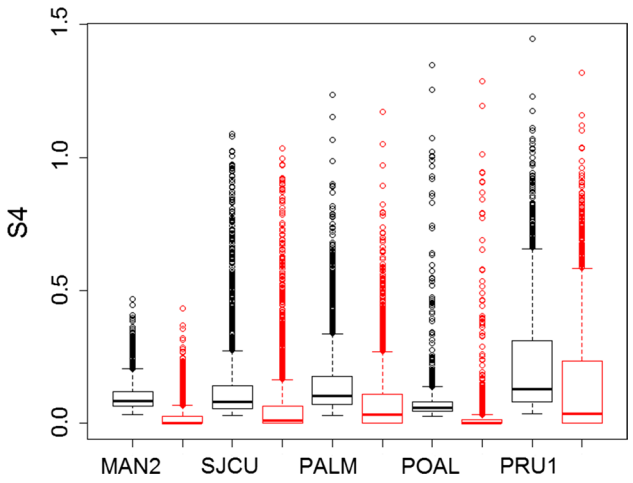

Fig. 10 Box plot of S_4 index of stations MAN2, SJCU, PALM, POAL and PRU1 without (black) and with (red) removal of sidereal-day effects (multipath)

We generated the skewness coefficients to S_4 time series (6 days data) on strong scintillation period before and after removing sidereal-day effects. Note that negative skewness indicates left-skewed distribution and positive skewness right-skewed one. Thus, the increase in the skewness coefficients with the multipath removal shows that the data became more asymmetric to the right (Table 2). This fact is expected considering that the S_4 values in the weak scintillation period, representing mostly multipath, rarely reached 0.5.

Figure 10 also shows that the station most and least influenced by scintillation is PRU1 and MAN2, respectively. This is in accordance with literature due to the EIA effect between 15° and 20° north and south magnetic latitude. Thus, the intensity of scintillation actually is weaker at the location of station MAN2 and more intensive at the location of station PRU1 (Fig. 1). Once station SJCU is located close to the EIA's crest, similarly to PRU1, it was expected that the scintillation effect would be strong at this station as well. The station POAL, which is not located in a region of intensive scintillation, presented a scintillation effect stronger than PALM and SJCU stations. However, although the maximum S_4 index at POAL (1.35) was higher than at PALM (1.24) and at SJCU (1.09), as shown in Fig. 10, only 1.2% of POAL observations exceeds the level of weak scintillation, as can be seen in Table 3. The percentage of S_4 index at PALM and SJCU stations that exceed the level 0.5 is higher than at POAL. This percentage is 4.2% to PALM and 5.9% to SJCU, which reduces to 2.4 and 4.7%, respectively, after multipath removal.

Table 2 Skewness coefficients for S_4 distribution without and with the sidereal-day effects (multipath) removal for all stations

Skewness	MAN2	SJCU	PALM	POAL	PRU1
S_4 without multipath removal	3.3	5.5	4.4	10.6	3.7
S_4 with multipath removal	7.9	6.7	5.8	16.1	4.4

Table 3 Percentage of observations that exceed the level of weak scintillation without and with multipath removal by station

Percentage	MAN2		SJCU		PALM		POAL		PRU1	
	Before	After	Before	After	Before	After	Before	After	Before	After
$S_4 \geq 0.5$	0.0	0.0	5.9	4.7	4.2	2.4	1.2	1.0	12.8	9.9
$S_4 \geq 0.7$	0.0	0.0	3.0	2.2	1.1	0.7	0.8	0.7	4.9	3.4
$0.5 \geq S_4 \geq 0.7$	0.0	0.0	2.9	2.5	3.0	1.7	0.4	0.3	7.9	6.5

Conclusions

The presence of a periodic behavior, which is typical of multipath effect, was verified in scintillation data using five stations from the CIGALA/CALIBRA network. From the wavelet decomposition of the scintillation S_4 index, it was possible to estimate and remove this identified periodic effect. We obtained a more realistic indicative S_4 index corrected from sidereal-day effects that better represents the scintillation and is useful to future investigations of scintillation effect.

It is noteworthy that for effective analysis of scintillation it is necessary to analyze each satellite and station because the scintillation effect is specific and depends on the location of both stations and satellites. The presented results are based on 6 days of data, which is the largest dataset allowing to check visually the presence of cyclic effects such as daily repeatability. The analysis made on this dataset is representative and could be extended to cover a season or a year. Using another dataset of 6 days would also not change the analysis.

Therefore, it follows that by multiscale wavelets analysis it is possible to take a first step into separating the scintillation effect from other sidereal-day effects, mainly multipath, that can influence the scintillation S_4 index analysis. For future work, the scales that were identified as the most important to characterize the scintillation effects should be investigated. Other scintillation indexes, such as phi60, should be evaluated to investigate the meaning of the identified periodicities such as those from 4 to 8 h and from 16 to 32 min.

Acknowledgements The author would like to thank FAPESP (Foundation for Research Support of the State of São Paulo) for the scholarship to the first author (FAPESP Process No. 2012/13362-5), CNPq for the financial support (Processes 304247/2012-0 and 473973/2012) and Projects CIGALA and CALIBRA (funded by the European Commission in the framework of the FP7-GALILEO-2009-GSA and FP7–GALILEO–2011–GSA–1a, respectively, and FAPESP Project No. 06/04008-2) for database.

Appendix: NDWT pyramid algorithm

Given a time series $\{X_t : t = 0, \ldots, N-1\}$, the result of the filtering of $\{X_t\}$ with the NDWT wavelet $\{\tilde{h}_k\}$ and scaling $\{\tilde{g}_k\}$ filters is given, respectively, by (Percival and Walden 2000)

$$\tilde{W}_{j,t} = \sum_{k=0}^{K-1} \tilde{h}_{j,k} X_{t-k \bmod N} \tag{5}$$

$$\tilde{V}_{j,t} = \sum_{k=0}^{K-1} \tilde{g}_{j,k} X_{t-k \bmod N}, \quad t = 0, 1, \ldots, N-1 \tag{6}$$

The two sequences given by (5) and (6), called NDWT wavelet and scaling coefficients, represent the NDWT of decomposition level j, and stipulate that the elements of $\tilde{W}_j$, $\tilde{V}_j$ and $\tilde{V}_{j-1}$ are obtained by circularly filtering of $\{X_t\}$ with the filters $\{\tilde{g}_{j,k}\}$, $\{\tilde{h}_{j,k}\}$ and $\{\tilde{h}_{j-1,k}\}$, respectively. The term "mod" from the equations refers to "maximal overlap discrete," that treats time series X as if it were circular, making X to be represented with the same number N of coefficients at each scale.

However, it is possible to obtain $\tilde{W}_j$ and $\tilde{V}_j$ by filtering of $\tilde{V}_{j-1}$ as in the following equation

$$\tilde{W}_{j,t} = \sum_{k=0}^{K-1} \tilde{h}_k \tilde{V}_{j-1,t-2^{j-1}k \bmod N} \tag{7}$$

$$\tilde{V}_{j,t} = \sum_{k=0}^{K-1} \tilde{g}_k \tilde{V}_{j-1,t-2^{j-1}k \bmod N}, \quad t = 0, 1, \ldots, N-1 \tag{8}$$

Equations (7) and (8) represent the NDWT pyramid algorithm, and they can be written in matrix form as

$$\tilde{W}_{j,t} = \tilde{B}_j \tilde{V}_{j-1} \text{ and } \tilde{V}_j = \tilde{A}_j \tilde{V}_{j-1} \tag{9}$$

where the rows of $\tilde{B}_j$ contain circularly shifted versions of $\{\tilde{h}_k\}$ after it has been upsampled to width $2^{j-1}(K-1)+1$, that consists of inserting 2^{j-1} zeros between each of the K values of the original filter, and then periodized to length

N, and with a similar construction for $\tilde{A}_j$ based upon $\{\tilde{g}_k\}$ (Percival and Walden 2000).

The NDWT also allows reconstructing $\tilde{V}_{j-1}$ from $\tilde{W}_j$ and $\tilde{V}_j$. The inverse NDWT acts to restore the signal in the time domain from its decomposition, and it can be calculated via inverse pyramidal algorithm described by the following equation,

$$\tilde{V}_{j-1,t} = \sum_{k=0}^{K-1} \tilde{h}_k \tilde{W}_{j,t+2^{j-1}k \bmod N} + \sum_{k=0}^{K-1} \tilde{g}_k \tilde{V}_{j,t+2^{j-1}k \bmod N}, \quad t = 0, 1, \ldots, N-1 \tag{10}$$

which can be expressed in matrix notation as

$$\tilde{V}_{j-1} = \tilde{B}_j^T \tilde{W}_j + \tilde{A}_j^T \tilde{V}_j \tag{11}$$

where $\tilde{B}_j^T$ and $\tilde{A}_j^T$ are transposed matrix of $\tilde{B}_j$ and $\tilde{A}_j$, respectively.

References

Brassarote GON, Souza EM, Monico JFG (2015) Multiscale analysis of GPS time series from non-decimated wavelet to investigate the effects of ionospheric scintillation. TEMA (São Carlos) 16(2):119–130

Briggs BH, Parkin IA (1963) On the variation of radio star and satellite scintillations with zenith angle. J Atmos Terr Phys 25(6):339–366

Camargo PO, Monico JFG, Ferreira LDD (2000) Application of ionospheric corrections in the equatorial region for L1 GPS users. Earth Planets Space 52(11):1083–1089

Davies K (1990) Ionospheric radio. Peter Peregrinus Ltd, London, p 580

Kelley MC (1989) The earths ionosphere: plasma physics and electrodynamics. Academic Press, San Diego

Kintner PM, Kil H, Beach TL, de Paula ER (2001) Fading timescales associated with GPS signals and potential consequences. Radio Sci 36(4):731–743

Kintner PM, Ledvina BM, de Paula ER (2007) GPS and ionospheric scintillations. Space. Weather 5:S09003. https://doi.org/10.1029/2006SW000260

Maini AK, Agrawal V (2007) Satellite technology: principles and applications. Wiley, India

Mallat SG (1989) A theory for multiresolution signal decomposition: the wavelet representation. IEEE Trans Pattern Anal 11(7):674–693

Materassi M, Alfonsi L, De Franceschi G, Romano V, Mitchell CN, Spalla P (2009) Detrend effect on the scalograms of GPS power scintillation. Adv Space Res 43(11):1740–1748

McNamara LF (1991) The ionosphere: communications, surveillance, and direction finding. Krieger publishing company, Malabar

Mushini SC, Jayachandran PT, Langley RB, Macdougall JW, Pokhotelov D (2012) Improved amplitude-and phase-scintillation indices derived from wavelet detrended high-latitude GPS data. GPS Solut 16(3):363–373

Nason GP (2008) Wavelet methods in statistics with R. Springer, New York

Percival DB, Walden AT (2000) Wavelets methods for time series analysis. Cambridge University Press, Cambridge

Starck JL, Murtagh F, Bertero M (2011) Starlet transform in astronomical data processing. In: Handbook of mathematical methods in imaging, Springer, New York, pp 1489–1531

Streets RBJ (1969) Variation of radio star and satellite scintillations with sunspot number and geomagnetic latitude. J Can Soc Expl Geophys 5:35–52

Tiwari R, Skone S, Tiwari S, Strangeways HJ (2011) 3WBMod Assisted PLL GPS software receiver for mitigating scintillation affect in high latitude region. In: IEEE General assembly and scientific symposium, 2011 XXXth URSI, pp 1–4

Tiwari R, Strangeways HJ, Tiwari S, Ahmed A (2013) Investigation of ionospheric irregularities and scintillation using TEC at high latitude. Adv Space Res 52(6):1111–1124

Vani BC, Shimabukuro MH, Monico JFG (2016) Visual exploration and analysis of ionospheric scintillation monitoring data: the ISMR query tool. Comput Geosci. https://doi.org/10.1016/j.cageo.2016.08.022

Gabriela de Oliveira Nascimento Brassarote received her B.Sc. in Mathematics at São Paulo State University (UNESP) in Presidente Prudente, Brazil, in 2011; Master in Computational and Applied Mathematics in 2014 and applied for the Ph.D. in Cartographic Science, starting in March 2015, both in UNESP. Her research activities involve multiscale wavelet analysis of time series, mainly GNSS signals.

Eniuce Menezes de Souza is a professor at Department of Statistics, Maringa State University (UEM). She received her B.Sc. degree in Mathematics in 2001 and her M.Sc. degree (2004) and Ph.D. in Cartographic Science (2008) from São Paulo State University (UNESP). Her research involves GNSS multipath and scintillation mitigation, multiscale wavelet analysis and applied statistics, mainly time series modeling.

João Francisco Galera Monico is a researcher level II at Department of Cartography, UNESP, Presidente Prudente. He received her B.Sc. degree in Cartographic Engineering from UNESP in 1982, M.Sc. in Geodetic Sciences from Paraná Federal University (1988), Ph.D. in 1995 from IESSG University of Nottingham. He has worked extensively with GNSS positioning, atmosphere monitoring, adjustment and quality control in geodesy and cartography.